Overcoming Resistance in Cancer Therapy: Computational Exploration of PIK3CA Mutations, Unveiling Novel Non-Toxic Inhibitors, and Molecular Insights Into Targeting PI3Kα

Ilham Kandoussi[1] (iD), Ghyzlane El Haddoumi[1], Mariam Mansouri[1], Lahcen Belyamani[2,3], Azeddine Ibrahimi[1] and Rachid Eljaoudi[1,2,3,4]

[1]Biotechnology Lab (MedBiotech), Bioinova Research Center, Rabat Medical & Pharmacy School, Mohammed V University in Rabat, Rabat, Morocco. [2]Mohammed VI University of Health Sciences (UM6SS), Casablanca, Morocco. [3]Emergency Department, Military Hospital Mohammed V, Medical and Pharmacy School, Mohammed V University in Rabat, Rabat, Morocco. [4]Department of Pharmacology and Toxicology, Faculty of Medicine and Pharmacy, Mohammed V University in Rabat, Rabat, Morocco.

ABSTRACT: Phosphoinositide-3-kinases (PI3K) are pivotal regulators of cell signaling implicated in various cancers. Particularly, mutations in the PIK3CA gene encoding the p110α catalytic subunit drive oncogenic signaling, making it an attractive therapeutic target. Our study conducted in silico exploration of 31 PIK3CA mutations across breast, endometrial, colon, and ovarian cancers, assessing their impacts on response to PI3Kα inhibitors and identifying potential non-toxic inhibitors and also elucidating their effects on protein stability and flexibility. Specifically, we observed significant alterations in the stability and flexibility of the PI3K protein induced by these mutations. Through molecular docking analysis, we evaluated the binding interactions between the selected inhibitors and the PI3K protein. The filtration of ligands involved calculating chemical descriptors, incorporating Veber and Lipinski rules, as well as IC50 values and toxicity predictions. This process reduced the initial dataset of 1394 ligands to 12 potential non-toxic inhibitors, and four reference inhibitors with significant biological activity in clinical trials were then chosen based on their physico-chemical properties. This analysis revealed Lig5's exceptional performance, exhibiting superior affinity and specificity compared to established reference inhibitors such as pictilisib. Lig5 formed robust binding interactions with the PI3K protein, suggesting its potential as a highly effective therapeutic agent against PI3K-driven cancers. Furthermore, molecular dynamics simulations provided valuable insights into Lig5's stability and its interactions with PI3K over 100 ns. These simulations supported Lig5's potential as a versatile inhibitor capable of effectively targeting various mutational profiles of PI3K, thereby mitigating issues related to resistance and toxicity commonly associated with current inhibitors.

KEYWORDS: Phosphoinositide-3-kinases, PIK3CA mutations, cancer, inhibitor screening, molecular docking, molecular dynamics simulation, personalized medicine

Introduction

Phosphoinositide-3-kinases (PI3K) are a family of lipid kinases that catalyze the phosphorylation of phosphoinositides at the 3'-hydroxyl group, regulating signaling pathways involved in cell proliferation, adhesion, survival, and motility.[1,2] They consist mainly of a p110 catalytic subunit and a p85 regulatory subunit and are divided according to the structural characteristics and the specificity of the substrates into three classes: PI3K class I, class II, and class III. PI3K class I is the most studied class in the search for therapeutic targets for various types of cancers, and it is divided into 2 subclasses PI3K class IA and PI3K class IB; PI3K class IA, they group together the p110α, p110β, and p110δ isoforms encoded by the PIK3CA, PIK3CB, and PIK3CD genes, respectively.[3,4] Mutations of PIK3CA are found in approximately 30% of human cancers and identified in a wide spectrum of tumors.[1,5] This gene is then considered the second most common mutated gene in all

cancers.[6] Most mutations are found near two positions in the helical or catalytic domains.[7] They have specific effects on downstream carcinogenic signals, and their coexistence leads to a synergistic enhancement of catalytic subunit activity.[8] This deregulation promotes cell proliferation and migration, glucose transport and catabolism, cytoskeletal rearrangement, and angiogenesis. This plays an important role in the initiation, progression, and maintenance of tumors.[9] PIK3CA represents one of the most mutated oncogenes identified in many types of human cancers, primarily breast, endometrial, colorectal, and ovarian cancer, and may be a useful diagnostic and therapeutic target[7,10-12] well known for precision cancer medicine.[6] Since PI3K is strongly implicated in cancer, much effort has been made to discover inhibitors, which could allosterically or competitively alter the activity of PI3K kinase.[13] Most PI3K inhibitors that have entered clinical development are reversible inhibitors and are Adenosine Triphosphate-competitive.[14] The

toxicities of these small-molecule PI3K inhibitors depend on the specificity of their isoforms. For example, PI3Kα inhibitors are mainly linked to skin rashes and hyperglycemia.[13] Targeted therapies have certainly opened up a promising avenue in clinical cancer medicine, but the mutational heterogeneity of cancer remains a limiting factor[15] because mutations at the targets can then alter the activities of the drugs. Therefore, certain drugs used in the treatment of cancer may not provide the same positive results for all patients.[6]

For example, in a phase I study, the clinical benefit ratio (CBR) of alpelisib was 44% in tumors with hotspot PIK3CA mutations vs 20% in patients with wild-type PIK3CA.[16] It is also noted that the selection of a specific population of patients with active PIK3CA mutations determines the efficacy of PI3K inhibitors.[13]

On the basis of these data and to elucidate the activities of competitive ATP inhibitors of PI3K on a plethora of mutations, our study sets itself as objectives the *in silico* exploration of PI3KCA mutations in relation to breast cancer; of the endometrium, colon, and ovary; their impacts on the response to the various reference treatments targeting the PI3Kα protein; as well as the identification of new potential non-toxic inhibitors.

Material and Methods

Assembly of PIK3CA mutations

Oncogenic activation of PIK3CA is recognized in various types of cancer including the four types mentioned above, which led us to build a database containing all mutations (Single Nucleotide Polymorphism (SNP) type; i.e. mutations by substitution of a single base) associated with the latter. ClinVar and The Cancer Genome Atlas Program (TCGA) were used as reference.[17,18]

TCGA allowed us to directly select the mutations related to the four types of cancer, which allowed us to have 178 mutations. As for ClinVar, we needed to filter the downloaded file containing 452 mutations according to the type of cancer sought and the clinical significance, and we therefore had 12 mutations. The whole made 190 mutations, and by eliminating the doubling, we kept 182 mutations. In a final filtration step, the mutations located far from the active site were eliminated for the smooth running of the following steps. We chose to analyze only mutations occurring at the helical and kinase domains. So, we had 100 mutations in total that we will use in the rest of the work.

Three-dimensional structures

The X-ray crystallographic structure of PI3Kα (PDB ID:7PG5) chain A with a resolution of 2.20 Å was obtained from the Protein Data Bank (PDB) database and a size of 1068 amino acids, representing the wild type.[19] The quality of this crystal has been improved by refining the loops with Swissmodel (Global Model Quality Estimation score of 0.85% and 96.61% of residues in favorable regions of the Ramachandran plot). Using the Chimera software, we were able to generate the different mutations based on the 3D structure of the wild type.[20]

Predicting the effects of mutations

Although we selected the mutations expressed in the types of cancers that we adopted in this study from the databases, we must also predict the effect of these mutations on the function of the protein. To do this, we used the following prediction web servers: SIFT, Polyphen-2, and MutPred2.[21-23]

We entered as input the different mutations that we have according to the modality implied by each predictor. The results of each were expressed differently (for SIFT: affect protein function/tolerated; for polyphen-2: probably damaging/possibly damaging/benign; for MutPred2: pathogenic/neutral). According to these data, we had to filter the mutations leaving only those that do not affect the function of the protein, and this is done by respecting the correlation between the three predictors.[21-23]

To assess the effect of missense variations on protein stability and flexibility, we used DynaMut, a web server, to analyze and visualize protein dynamics by sampling conformations and assess the impact of mutations on protein dynamics and stability resulting from changes in vibrational entropy.[24]

Reference inhibitors collection

From the literature, the following inhibitors were chosen as reference inhibitors, and their properties will be used as the base to define the best inhibitor for PIK3CA:

- Alpelisib (BYL-719): a specific inhibitor of the class I PI3Kα isoform used in the treatment of breast cancer.[25]
- Copanlisib: a Pan-PI3K inhibitor in clinical phase II for the treatment of endometrial and ovarian cancer (NCT05082025).[26]
- Pictilisib (GDC-0941): a phase I pan-PI3K inhibitor for the treatment of solid tumors (NCT00876109).[27]
- Inavolisib (GDC-0077): selective PI3Kα inhibitor in clinical phase I/II for the treatment of solid tumors NCT04486352, NCT03006172, NCT04929223, and others.[26]

After identifying them, their 3D structures were downloaded from PubChem in SDF format and then converted to PDB format using Open Babel software.

Collection and filtration of potential inhibitors

The reference inhibitors were imported from the BindingDB database by a number of 1394. Subsequently, they were filtered according to several criteria; starting with the IC50, the inhibitors must have an IC50 value lower than that of the reference

inhibitors, that is, it must be less than or equal to 5 nM, which gives 111 inhibitors. Then, in a second filtration, the potential inhibitors must follow the rules of Lipinski's 5. At this stage, we had 30 potential inhibitors. Finally, we filtered the rest according to the rules of Veber to have 23 inhibitors in total after eliminating duplicates. As for the reference inhibitors, the SDF files of 3D structures of the potential inhibitors were downloaded again from the PubChem database, and they were subsequently converted into PDB format by Open Babel.[28,29]

The evaluation of the toxicity of the 23 potential inhibitors was carried out by the StopTox web server, which made it possible to determine 12 potential non-toxic inhibitors that will be prepared thereafter for the molecular docking stage.[30] The test was thus carried out to reference inhibitors, including pictilisib and inavolisib, which were not toxic, as was the case for alpelisib and copanlisib.

Docking and scoring

The filtered compounds were docked in the ATP site at the kinase domain of PI3K, and the key residues were determined from the literature, including M772, S774, K802, D810, Y836, E849, V851, S854, Q859, M922, and Ile932.[31] AutoDock 1.5.7.24 allowed the grid box to be prepared, with a spacing of 1Å and center coordinates set to X = –2.144 Å, Y = –8.122Å, Z = 19.129Å, with a size of X = 20Å, Y = 22Å, Z = 20Å. AutoDock Vina was used to assess binding affinity and conformation of selected ligands. This program allows docking of flexible ligands with about a dozen torsional degrees of freedom, and the empirical free-energy force field provides predicted energies ranked according to their magnitude generated in poses.[32,33]

Ligand-based pharmacophore modeling

Three-dimensional pharmacophores serve as valuable queries for retrieving potential lead compounds from structural databases, identifying molecules with specific desired attributes, and assessing similarity.[34]

To understand the affinity variations observed in the docking results between reference inhibitors and potential inhibitors, we generated a pharmacophore. This pharmacophore allows us to identify the structural features essential for the interaction with PI3Kα in reference inhibitors. In addition, we analyzed the root mean square deviation (RMSD) of the potential inhibitors to elucidate their structural differences compared to the reference inhibitors.

To construct the pharmacophore model, the training set was formed using flexible alignment of the four reference molecules (alpelisib, copanlisib, pictilisib, and inavolisib). In addition, the test set comprised the 12 molecules identified through docking as possessing favorable affinities. This method relies on 3D research distances between features, such as Hydrogen Bond Donor (HBD), Hydrogen Bond Acceptor (HBA), Aromatic

(Aro), and Hydrophobic (HyD), common among active compounds. The selected compounds underwent energy optimization and minimization through flexible alignment.

Two-dimensional interaction analysis

To comprehend the influence of structural variances between the optimal reference ligand and the most promising potential ligand, we conducted a 2D interaction analysis using the BioVia Discovery Studio 2019 software. This analysis focused on the interactions between pictilisib and Lig5 with wild-type PI3K, as well as PI3K carrying the Y1020C mutation found in various cancer types.

Molecular dynamics simulations

After comprehending the fixed docking of the ligand-protein complex, we proceeded to investigate its flexible docking through molecular dynamics (MD) simulations, aiming to emulate biological behavior. Two ligands were selected based on their docking score and free binding energy for further MD simulations; Lig5: the best potential inhibitor, and pictilisib: the best reference inhibitor.

MD simulations, spanning 100 ns, were conducted using Desmond, developed by Schrödinger LLC.[35,36] These simulations employ Newton's classical equation of motion to track atom movements over time.[37,38]

The receptor-ligand complex underwent preprocessing via the Protein Preparation Wizard of Maestro, entailing complex optimization and minimization. System preparation involved the use of the System Builder tool. The Transferable Intermolecular Interaction Potential 3 Points (TIP3P) solvent model within an orthorhombic box was selected. The OPLS 2005 force field was applied during the simulation.[39] Neutral models were achieved through the introduction of counter ions. To simulate physiological conditions, 0.15 M sodium chloride (NaCl) was added. The NPT ensemble was utilized, maintaining a temperature of 300K and pressure of 1 atm throughout the simulation. Prior to the simulation, models underwent relaxation. Trajectories were saved for examination every 100 ps, with simulation stability verified by comparing the RMSD of the protein and ligand over time.

Results

Mutational effect prediction

The 100 mutations filtered from the ClinVar and TCGA database, which were the subject of our study, were the subject of a study to predict the mutational effects on the function of the protein using three predictive tools, namely SIFT, Polyphene-2, and MutPred2, giving 31 deleterious mutations against 69 neutral mutations (Figure 1).

Only the 31 deleterious mutations with concordant results were considered and then distributed according to the type of
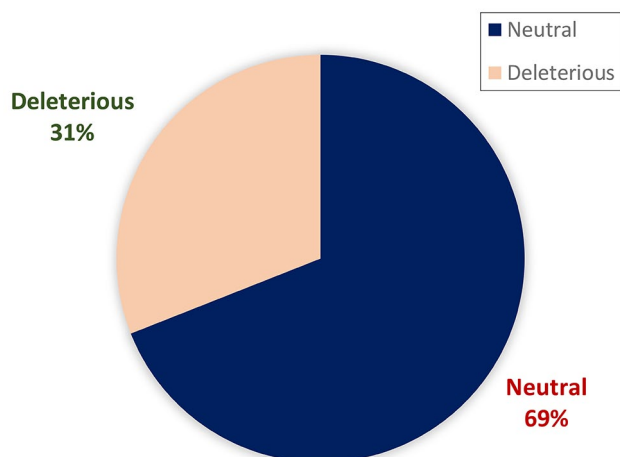
Figure 1. The result of the prediction of the effects of mutations.

cancer in which they are involved (Table 1), thus showing that the majority are linked to cancer from the endometrium, then from the breast, from the colon, and finally from the ovary with a single mutation (Figure 2), with the involvement of certain mutations in the four types of cancer studied indicated in bold in Table 1.

Study of stability and flexibility

The 31 mutations predicted as deleterious were investigated for their impacts on the stability and flexibility of the PI3Kα protein. The results show that the majority of mutations significantly increase stability while decreasing flexibility except mutations L658F, F684L, F1002L, Y1021C, and Y1021H, which are found to decrease both parameters at the same time. We also note that the mutation causing the most decrease in flexibility is G914R and that increasing stability the most is E600V (Figure 3).

Filtration of ligands

The filtration of the ligands was made by calculating the descriptors by the MOE software taking into consideration the rules of Veber and Lipinski (Table 2), and the IC50, which made it possible to go from 1394 to 23 potential inhibitors, has chosen as a reference four inhibitors that have shown significant biological activity during clinical trials, taking into consideration their physico-chemical properties.

The toxicity test carried out by StopTox revealed 12 potential non-toxic inhibitors (Table 3). This test, also carried out for the reference inhibitors, showed that the two inhibitors pictilisib (R1) and inavolisib (R3) did not show acute oral toxicity, unlike copanlisib (R2) and alpelisib (R4).

Molecular docking and scoring

The multi-docking result shows the calculated affinity in kcal/mol of the 12 potential inhibitors for wild-type 7PG5 and for

Table 1. Distribution of deleterious mutations according to the type of cancer.

PIK3CA deleterious mutations in endometrial cancer			
Y1021 C	**C901 F**	**P539 R**	**E600 K**
E542 V	R992 P	G903E	P953 S
Y1021 H	Q643 H	L929M	E600 V
F1002 L	F684 L	R818 H	F930 V
G914R	S576Y	R617 W	R818 C
M1004 V	M1004R		
PIK3CA deleterious mutations in breast cancer			
Y1021 C	**C901 F**	**P539 R**	**E600 K**
T957 P	L766 F	S629 C	**E545 V**
G914R			
PIK3CA deleterious mutations in colon cancer			
Y1021 C	R777 M	F945 C	L658 F
E545 V			
PIK3CA deleterious mutations in ovarian cancer			
E849 K			

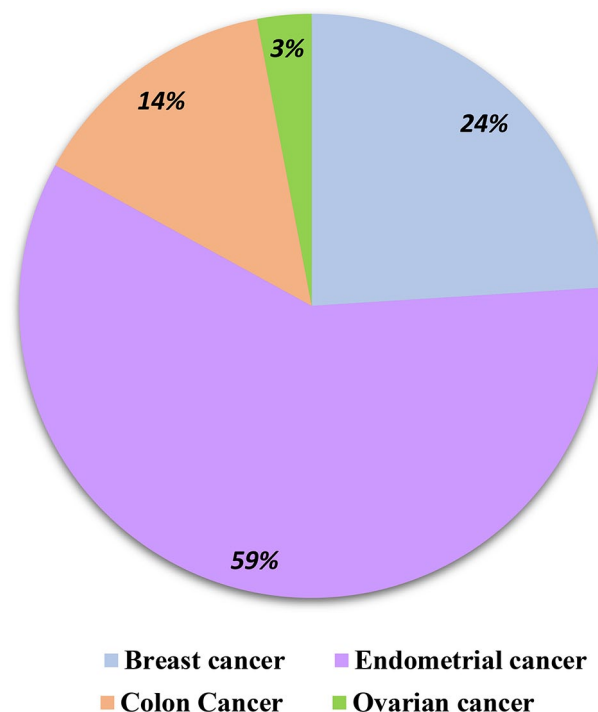The mutations marked in bold are those repeated in the different types of cancers studied.

Figure 2. The frequency of deleterious mutations in the PIK3CA protein in the four types of cancer.

the different PIK3CA mutations in breast cancer (Table 4), endometrial cancer (Table 5), colon cancer (Table 6), and ovarian cancer (Table 7), compared to that of the four reference
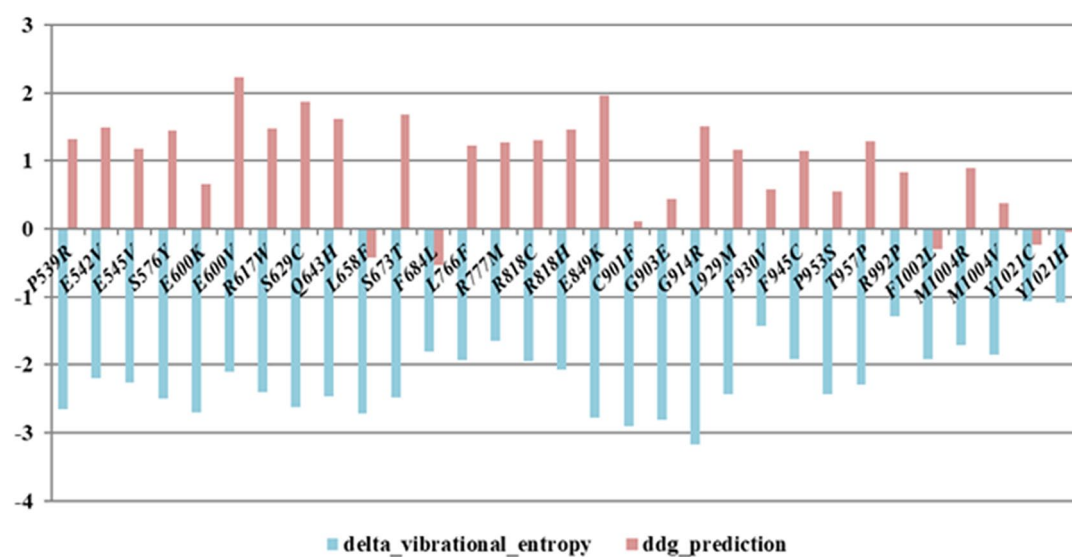
Figure 3. Impact of mutations on stability and flexibility of PI3K protein.

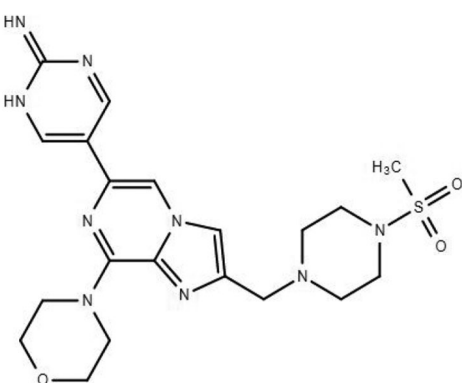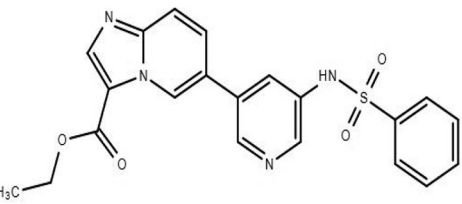**Table 2.** The physico-chemical properties of potential inhibitors.

INHIBITORS PUBCHEM ID	MOLECULAR WEIGHT (G/MOL)	IC50 (NM)	LOG P	NUMBER OF HYDROGEN DONORS	NUMBER OF HYDROGEN RECEPTORS	NUMBER OF ROTARY BONDS	POLAR SURFACE
9884685	348.362	2	2.031	1	5	2	84.52
25023741	370.47699	3	2.399	1	5	4	61.73
25023742	414.53	4	2.317	1	6	7	70.949
11647372	417.41998	5	0.583	0	6	4	81.43
52936849	422.465	1.1	2.253	1	5	7	103.18
137653212	426.47998	0.57	2.802	2	5	6	92.269
312145	428.43999	1.2	1.437	0	5	6	109.11
137642764	446.48999	0.5	0.361	1	5	3	97.69
145973569	461.93298	1	4.359	3	6	5	100.63
141461667	462.92099	1	4.178	3	7	5	113.52
137641601	468.517	2.9	2.655	2	6	7	109.34
137657573	470.53299	4.1	1.977	3	6	8	112.5
137656416	470.53299	1.9	2.369	3	6	8	112.5
135197572	472.47198	1.2	3.461	1	6	6	103.3
46927938	473.56198	2.3	−2.958	1	8	5	135.08
52917608	474.5	1.3	−0.058	1	6	4	114.76
145966764	479.923	1	4.512	3	6	5	100.63
145977475	479.923	1	4.512	3	6	5	100.63
137637213	482.54398	3.3	3.130	2	6	8	109.34
137656901	483.54398	2.5	1.702	3	6	8	121.37

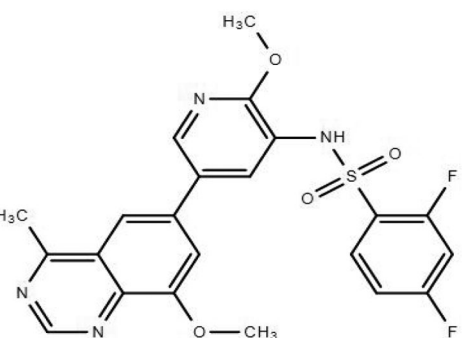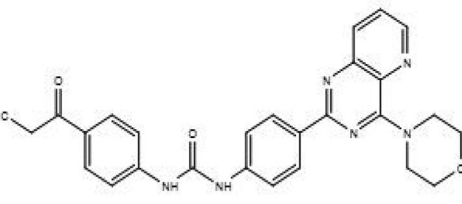*(Continued)*

Table 2. (Continued)
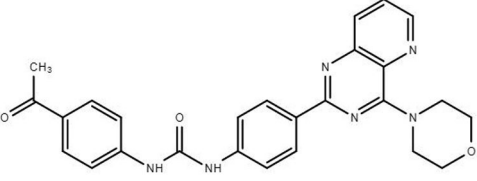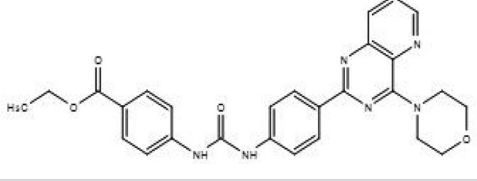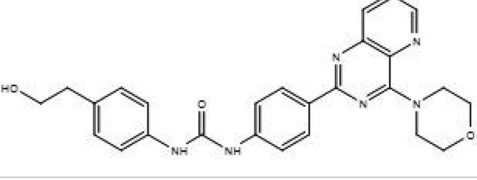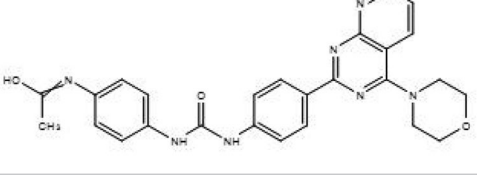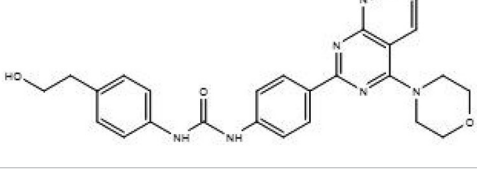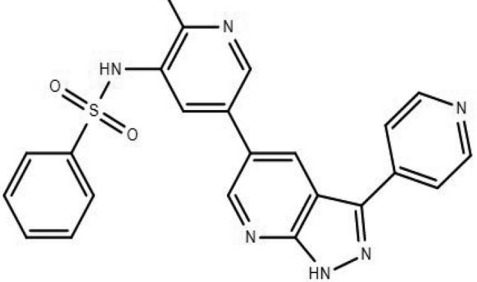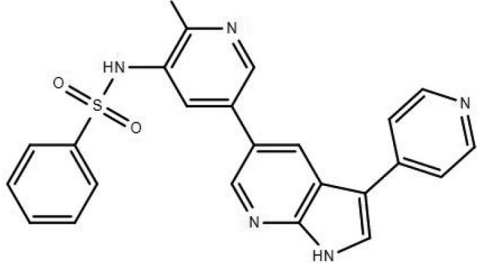
INHIBITORS PUBCHEM ID	MOLECULAR WEIGHT (G/MOL)	IC50 (NM)	LOG P	NUMBER OF HYDROGEN DONORS	NUMBER OF HYDROGEN RECEPTORS	NUMBER OF ROTARY BONDS	POLAR SURFACE
70689024	487.58899	2.6	−2.497	1	8	5	135.08
155512538	498.47	0.23	3.090	1	6	6	125.03
137648104	498.543	1.7	3.084	2	6	9	118.57
Alpelisib	441.5	5	3.2	2	8	4	129
Copanlisib	480.5	0.5	0.3	2	9	7	140
Pictilisib	513.6	3	1.6	1	10	5	144
Inavolisib	407.4	0.038	1.5	2	8	5	112

Table 3. Potential non-toxic inhibitors, chemical structure, and toxicity of reference inhibitors.

INHIBITORS	PUBCHEM ID	CHEMICAL STRUCTURE	ACUTE ORAL TOXICITY
Lig1	46927938		Non-toxic (−)
Lig2	52936849		Non-toxic (−)
Lig3	135197572		Non-toxic (−)
Lig4	137637213		Non-toxic (−)

(Continued)

Table 3. (Continued)

INHIBITORS	PUBCHEM ID	CHEMICAL STRUCTURE	ACUTE ORAL TOXICITY
Lig5	137641601		Non-toxic (–)
Lig6	137648104		Non-toxic (–)
Lig7	137656416		Non-toxic (–)
Lig8	137656901		Non-toxic (–)
Lig9	137657573		Non-toxic (–)
Lig10	141461667		Non-toxic (–)
Lig11	145973569		Non-toxic (–)

(Continued)

Table 3. (Continued)
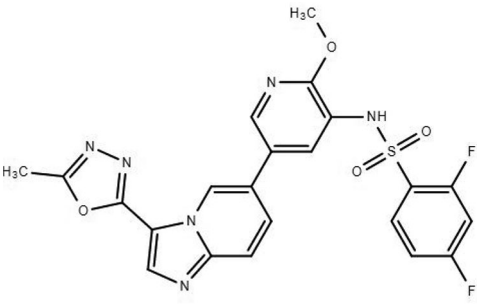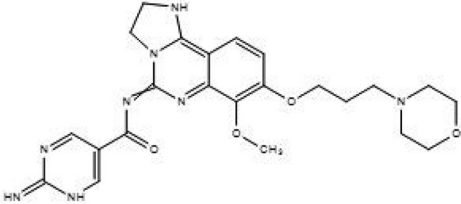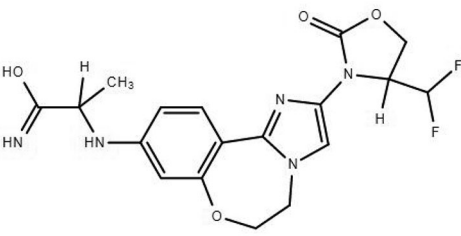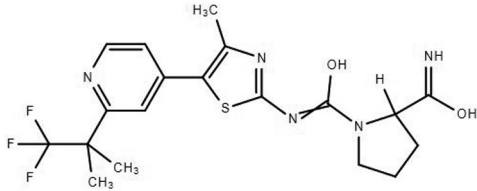
INHIBITORS	PUBCHEM ID	CHEMICAL STRUCTURE	ACUTE ORAL TOXICITY
Lig12	155512538		Non-toxic (−)
R1	17755052		Non-toxic (−)
R2	135565596		Toxic (+)
R3	124173720		Non-toxic (−)
R4	56649450		Toxic (+)

Table 4. Docking results referred to breast cancer.

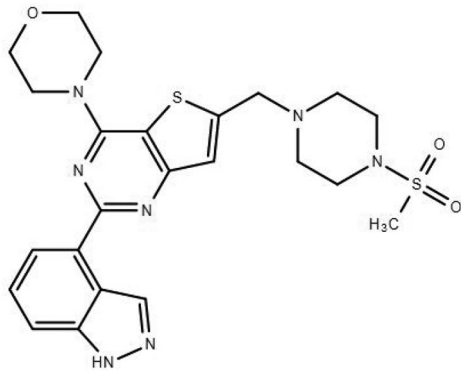| TARGETS	R1	R2	R3	R4	LIG1	LIG2	LIG3	LIG4	LIG5	LIG6	LIG7	LIG8	LIG9	LIG10	LIG11	LIG12
7pg5	–8,8	–8,1	–8,7	–8,4	–7,9	–8,1	–8,7	–9,0	**–9,2**	–8,8	–8,7	–9,0	–8,5	–8,2	–8,2	–8,9
C901F	–8,6	–7,8	–8,6	–8,2	–7,9	–8,1	–8,7	–9,0	**–9,2**	–8,8	–9,0	–9,1	–8,7	–8,2	–8,3	–9,0
E545V	–8,6	–7,8	–8,7	–8,2	–7,9	–8,1	–8,7	–9,0	**–9,3**	–8,8	–9,1	–8,8	–8,6	–8,1	–8,3	–9,0
E600K	–8,8	–7,9	–8,7	–8,3	–8,0	–7,8	–8,6	–9,0	**–9,2**	–8,8	–9,0	–8,8	–8,6	–8,2	–8,3	–9,0
S673T	–8,6	–7,9	–8,7	–8,2	–8,0	–8,1	–8,7	–9,0	**–9,2**	–8,8	–9,0	–8,8	–8,6	–8,2	–8,2	–9,0
T957P	–8,8	–8,2	–8,7	–8,3	–7,9	–8,0	–8,7	–9,0	**–9,3**	–8,8	–9,0	–9,4	–8,4	–8,2	–8,3	–9,0
S629C	–8,8	–7,7	–8,7	–8,3	–7,9	–8,2	–8,7	–9,0	**–9,3**	–8,8	–9,1	–9,4	–8,3	–8,1	–8,3	–9,0
L766F	–8,8	–7,7	–8,7	–8,2	–8,0	–8,0	–8,7	–9,0	**–9,2**	–8,8	–8,7	–9,3	–8,4	–8,1	–8,3	–9,0
P539R	–8,8	–8,1	–8,7	–8,3	–7,9	–8,1	–8,7	–9,0	**–9,3**	–8,8	–8,7	–8,8	–8,6	–8,2	–8,3	–9,0
G914R	–8,8	–8,3	–8,7	–8,4	–8,0	–8,3	–8,6	–9,0	**–9,3**	–8,8	–8,9	–8,8	–8,6	–8,2	–8,3	–9,0
Y1021C	–8,7	–8,3	–8,7	–8,3	–8,0	–8,1	–8,7	–9,0	**–9,2**	–8,8	–8,9	–9,3	–8,6	–8,1	–8,3	–9,0

The inhibitors marked in bold correspond to the inhibitors with the best affinity for the different targets.

inhibitors. The results show that the Lig5 inhibitor has a better affinity toward the wild protein as well as all the mutated models varying between –9 and –9.3 Kcal/mol, and this compared to the reference inhibitors, including pictilisib, is the non-toxic inhibitor with the best affinity

Pharmacophore model result

The flexible alignment results of the four reference ligands, forming the training set, revealed a pharmacophore map comprising three distinct features denoted as F1: Acc and ML, F2: ML│Aro│Acc│Don, and F3: ML│Hyd│Don; the distance between each feature is illustrated in Table 8. The graphical representation of the model outcomes is depicted in Figure 4A, offering a comprehensive visualization of the spatial arrangement of these crucial features. Detailed inter-feature distances are elucidated in Table 8, providing a quantitative analysis of essential intermolecular relationships. Furthermore, the spatial distribution of distances between the different pharmacophore features is graphically represented in Figure 4B. Subsequently, the screening results of the test set formed by the 12 potential inhibitors showing better affinities than the reference inhibitors during molecular docking indicated that Lig1 emerged as the most optimal ligand with an RMSD value of 0.30, while Lig5, exhibiting a high docking score, displayed an RMSD value of 0.40. Both results are visually presented in Figure 5A and B, respectively, providing insights into the structural aspects and potential binding affinities of the ligands.

Two-dimensional interaction analysis of pictilisib and Lig5 with wild-type and mutant PI3 K

Analysis of 2D interactions shows that Lig5 makes two hydrogen bonds with S854 and V851, an additional bond with K802, a pi-sulfur interaction with C838, and a T-shaped pi-pi interaction with W780 (Figure 6). In addition, it forms pi-alkyl interactions with I932 and I848, demonstrating its adaptability to different molecular environments. In contrast, pictilisib relies primarily on T-shaped pi-alkyl and pi-pi interactions, but in less variety.

Molecular Dynamics

In the realm of bodily functions, proteins do not stay still to receive ligands at their receptors. Instead, they undergo continual random conformational changes, necessitating flexible docking of both the protein and ligand. MD simulations aid in flexible docking by employing Newtonian physics to replicate atomic-scale movements. These simulations occur within dynamic solvent environments, closely resembling physiological systems. In this study, an MD simulation was carried out for the ligand, indicating the best docking score for the wild protein and the mutated models. Lig5 was analyzed compared to Pictilisib, having shown the best docking score among the reference inhibitors included in our study.

Table 5. Docking results referred to endometrial cancer.

TARGETS	R1	R2	R3	R4	LIG1	LIG2	LIG3	LIG4	LIG5	LIG6	LIG7	LIG8	LIG9	LIG10	LIG11	LIG12
7pg5	−8,8	−8,1	−8,7	−8,4	−7,9	−8,1	−8,7	−9,0	**−9,2**	−8,8	−8,7	−9,0	−8,5	−8,2	−8,2	−8,9
C901F	−8,6	−7,8	−8,6	−8,2	−7,9	−8,1	−8,7	−9,0	**−9,2**	−8,8	−9,0	−9,1	−8,7	−8,2	−8,3	−9,0
E600K	−8,8	−7,9	−8,7	−8,3	−8,0	−7,8	−8,6	−9,0	**−9,2**	−8,8	−9,0	−8,8	−8,6	−8,2	−8,3	−9,0
E600V	−8,5	−8,3	−8,9	−8,1	−7,5	−7,2	−8,5	−8,8	**−9,0**	−8,6	−8,7	−8,6	−8,3	−7,9	−8,5	−8,3
F930V	−8,4	−8,0	−8,4	−8,2	−7,8	−8,0	−8,5	−8,9	**−9,1**	−8,7	−8,7	−8,6	−8,4	−8,0	−8,1	−8,8
F1002L	−8,5	−7,9	−8,9	−8,2	−7,4	−7,2	−8,5	−8,8	**−9,0**	−8,6	−8,8	−8,6	−8,0	−7,9	−8,5	−8,2
G903E	−8,8	−8,0	−8,7	−8,0	−8,0	−8,1	−8,7	−9,0	**−9,2**	−8,8	−8,7	−8,8	−8,7	−8,1	−8,2	−9,0
L929M	−8,8	−8,2	−8,7	−8,1	−8,0	−8,0	−8,7	−9,0	**−9,2**	−8,8	−9,1	−9,3	−8,7	−8,1	−8,3	−8,9
M1004R	−8,8	−8,3	−8,7	−8,2	−7,9	−8,0	−8,7	−9,0	**−9,2**	−8,8	−9,1	−9,4	−8,5	−8,2	−8,3	−9,0
M1004V	−8,8	−8,3	−8,6	−8,2	−7,9	−8,2	−8,6	−9,0	**−9,2**	−8,8	−8,6	−9,5	−8,5	−8,2	−8,3	−9,0
P539R	−8,8	−8,1	−8,7	−8,3	−7,9	−8,1	−8,7	−9,0	**−9,3**	−8,8	−8,7	−8,8	−8,6	−8,2	−8,3	−9,0
P953S	−8,8	−8,2	−8,7	−8,1	−7,9	−8,1	−8,7	−9,0	**−9,3**	−8,8	−8,7	−8,8	−8,6	−8,2	−8,3	−9,0
Q643H	−8,6	−7,9	−8,7	−8,3	−8,0	−8,1	−8,7	−9,0	**−9,2**	−8,8	−8,8	−8,8	−8,5	−8,2	−8,3	−9,0
R617W	−8,6	−8,2	−8,6	−8,2	−7,9	−8,1	−8,7	−9,0	**−9,3**	−8,8	−9,1	−8,8	−8,5	−8,1	−8,3	−9,0
R818C	−8,8	−8,3	−8,7	−8,3	−7,9	−8,1	−8,7	−9,0	**−9,3**	−8,8	−9,1	−8,8	−8,7	−8,1	−8,3	−9,0
R818H	−8,8	−8,2	−8,6	−8,2	−8,0	−8,3	−8,7	−9,0	**−9,2**	−8,8	−9,1	−9,3	−8,7	−8,1	−8,3	−9,0
R992P	−8,9	−7,9	−8,7	−8,3	−8,0	−8,2	−8,7	−9,0	**−9,2**	−8,8	−9,1	−8,8	−8,5	−8,2	−8,3	−8,9
S576Y	−8,8	−7,6	−8,7	−8,2	−7,9	−8,1	−8,7	−9,0	**−9,2**	−8,8	−8,7	−9,4	−8,6	−8,1	−8,3	−9,0
Y1021C	−8,7	−8,3	−8,7	−8,3	−8,0	−8,1	−8,7	−9,0	**−9,2**	−8,8	−8,9	−9,3	−8,6	−8,1	−8,3	−9,0
Y1021H	−8,8	−7,9	−8,7	−8,2	−7,9	−8,1	−8,6	−9,0	**−9,2**	−8,8	−8,7	−8,8	−8,7	−8,2	−8,3	−9,0
E542V	−8,8	−8	−8,7	−8,1	−7,9	−8,1	−8,6	−9,0	**−9,2**	−8,8	−8,7	−9,4	−8,5	−8,2	−8,3	−9,0
G914R	−8,8	−8,3	−8,7	−8,4	−8,0	−8,3	−8,6	−9,0	**−9,3**	−8,8	−8,9	−8,8	−8,6	−8,2	−8,3	−9,0
F684L	−8,8	−7,5	−8,7	−8,1	−7,9	−8,1	−8,7	−9,0	**−9,2**	−8,8	−8,7	−8,8	−8,4	−8,1	−8,3	−9,0

The inhibitors marked in bold correspond to the inhibitors with the best affinity for the different targets.

Table 6. Docking results referred to colon cancer.

TARGETS	R1	R2	R3	R4	LIG1	LIG2	LIG3	LIG4	LIG5	LIG6	LIG7	LIG8	LIG9	LIG10	LIG11	LIG12
7pg5	−8,8	−8,1	−8,4	−8,7	−7,9	−8,1	−8,7	−9,0	**−9,2**	−8,8	−8,7	−9	−8,5	−8,2	−8,2	−8,9
F945C	−8,8	−8,3	−8,2	−8,7	−7,9	−8,2	−8,6	−9,0	**−9,2**	−8,8	−9,1	−8,8	−8,5	−8,1	−8,1	−9,0
L658F	−8,6	−8,3	−8,4	−8,6	−8,0	−8,0	−8,7	−9,0	**−9,2**	−8,8	−8,7	−9,3	−8,5	−8,1	−8,3	−9,0
R777M	−8,8	−8,1	−8,3	−8,7	−7,9	−8,2	−8,7	−9,0	**−9,2**	−8,7	−9	−8,8	−8,7	−8,1	−8,3	−8,9
Y1021C	−8,7	−8,3	−8,3	−8,7	−8,0	−8,1	−8,7	−9,0	**−9,2**	−8,8	−8,9	−9,3	−8,6	−8,1	−8,3	−9,0
E545V	−8,6	−7,8	−8,2	−8,7	−7,9	−8,1	−8,7	−9,0	**−9,3**	−8,8	−9,1	−8,8	−8,6	−8,1	−8,3	−9,0

The inhibitors marked in bold correspond to the inhibitors with the best affinity for the different targets.

Table 7. Docking results referred to ovarian cancer.

TARGETS	R1	R2	R3	R4	LIG1	LIG2	LIG3	LIG4	LIG5	LIG6	LIG7	LIG8	LIG9	LIG10	LIG11	LIG12
7pg5	−8,8	−8,1	−8,4	−8,7	−7,9	−8,1	−8,7	−9,0	**−9,2**	−8,8	−8,7	−9,0	−8,5	−8,2	−8,2	−8,9
E849K	−8,6	−7,5	−8,1	−8,7	−7,9	−8,1	−8,7	−9,0	**−9,2**	−8,8	−8,6	−8,8	−8,5	−8,1	−8,3	−8,9

The inhibitors marked in bold correspond to the inhibitors with the best affinity for the different targets.

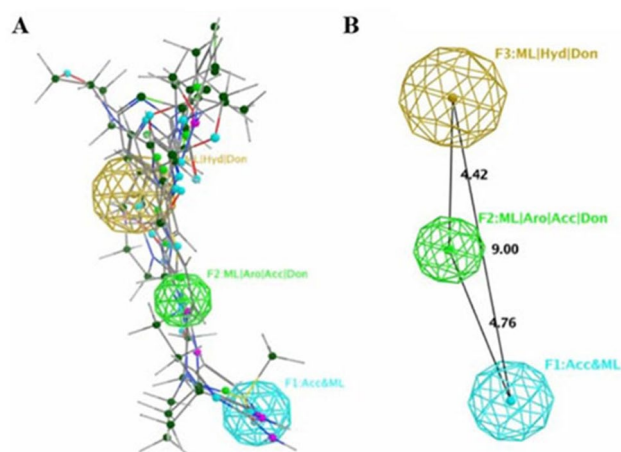**Table 8.** Distances between pharmacophore features.

	F1: ACC AND ML	F2: ML | ARO | ACC | DON	F3: ML | HYD | DON
F1: Acc and ML	0 Å	4,76 Å	9,00 Å
F2: ML | Aro | Acc | Don	4,76	0 Å	4,42 Å
F3: ML | Hyd | Don	9,00 Å	4,42 Å	0 Å

Figure 4. The 3D pharmacophore model. (A) Result obtained after flexible alignment. (B) Distances between individual features in the pharmacophore model, represented in Angstrom units.
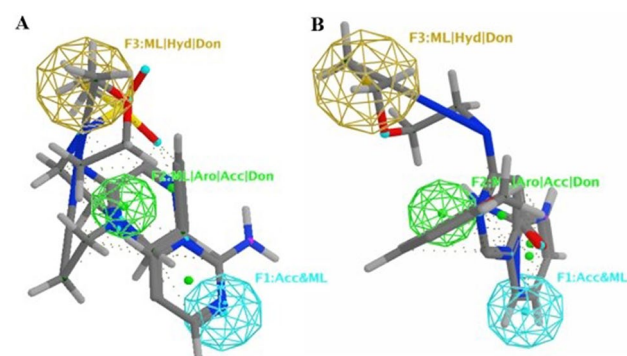

Figure 5. The pharmacophore model features. (A) Screening of the map with the reference ligand. (B) Screening of the map with Lig5.

Analysis of RMSD value of proteins and ligands

The MD simulation results were scrutinized by assessing the RMSD values of both Cα and ligands. RMSD, or RMSD, serves as an indicator of the extent of conformational alterations undergone by the protein and ligand from their initial structures throughout the simulation.

The current study involved conducting MD simulations focusing on the optimal ligand (Lig5) in comparison to the standard pictilisib-PI3Kα complex. Upon analyzing the data from the simulation interaction diagram, it was noted that the RMSD of the Lig5-PI3Ka complex displayed fluctuations ranging from 2 to 3 Å. In contrast, the pictilisib-PI3 K complex exhibited fluctuations ranging from 4.5 to 10.5 Å relative to the initial frame over the course of the trajectory (Figure 7A and B).

Analysis of RMSF value of proteins and ligands

Root mean square fluctuations (RMSF) aid in identifying local variations within the protein structure. They were employed to pinpoint the specific residues responsible for structural fluctuations within the complex. Reduced fluctuations indicate greater stability. Peaks signify regions of proteins that experienced the highest fluctuations during the simulations.[40] In the case of the two complexes under study, Lig5-PI3 K and pictilisib-PI3 K, it is observed that the N-terminal tails (comprising the first 200 residues) exhibit comparatively lower fluctuations, typically not

exceeding 2 Å. Conversely, the region between residue 200 and 550 demonstrates more pronounced fluctuations, reaching up to 5.5 Å, with more prominent peaks observed in the Lig5-PI3 K complex. Thus, it is notable that in both complexes, interactions predominantly occur at the level of the kinase domain (Figure 7C and D).

Analysis of gyration, SASA value of protein and ligand RMSF

Gyration analysis is a method utilized in MD simulations to assess the compactness or spatial distribution of a molecular system over time. It involves calculating the radius of gyration, which quantifies the spread of mass or atoms within a molecule from its center of mass. This analysis provides insights into the overall shape and conformational dynamics of the molecule throughout the simulation. Gyration analysis helps researchers understand how a molecule or biomolecular complex behaves and changes its structure under different conditions or interactions. The Rg value was computed over a 100-ns trajectory and juxtaposed with the simulation time illustrated in Figure 7E. The findings indicated that the lig5-PI3 K system exhibited a higher Rg value than the pictilisib-PI3 K complex, particularly within the initial 40 ns, before displaying an inverse trend thereafter. Primarily, the system demonstrated favorable compactness (33.5 ± 0.3 Å); however, post 40 ns, the Rg value gradually declined to (33.0 ± 0.3 Å). In contrast, the pictilisib-PI3 K system displayed fewer structural alterations and maintained a consistently stable Rg value (33.18 ± 0.12 Å).

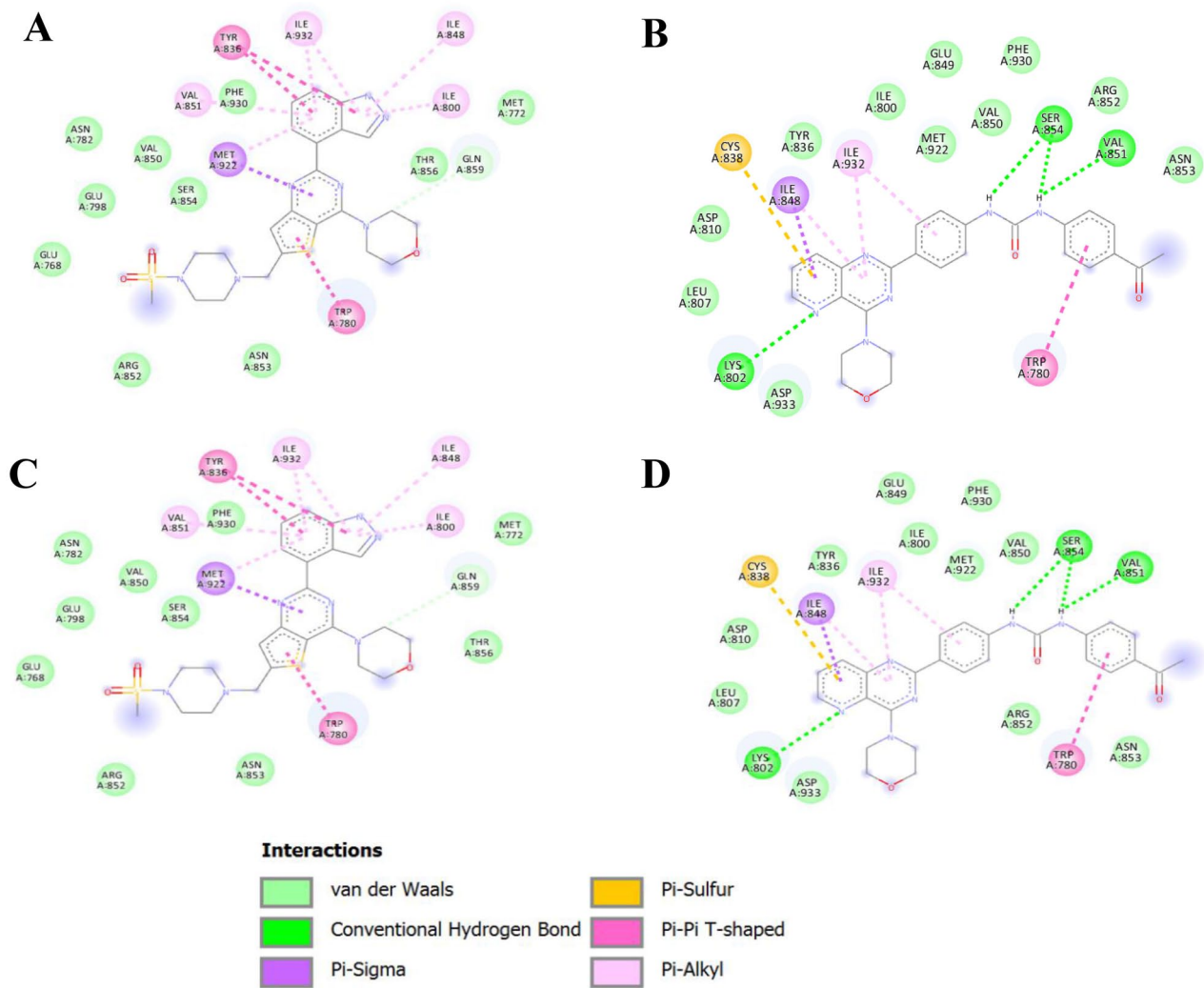The solvent-accessible surface area (SASA) is a measure of the surface area of a biomolecule that is accessible to the

Figure 6. Two-dimensional interaction analysis of pictilisib and Lig5 with wild-type and Y1020C mutant PI3 K. (A) PICTILISIB WT. (B) LIG5 WT. (C) PICTILISIB MUT. (D) LI5-MUT.

surrounding solvent molecules. It is an important parameter in the study of protein folding, ligand binding, and other biological processes. SASA denotes the extent of interaction between complexes and solvents, thereby indicating conformational alterations during interactions. The SASA values for Lig5-PI3 K and pictilisib-PI3 K were recorded as 48032.97A ± 690.36 and 47387.95A ± 557.28, respectively (Figure 7F).

The average RMSF of Lig5 measured 1.07 Å, while the mean RMSF for pictilisib was 3.55 Å (Figure 7G and H). These findings indicate a reduced level of fluctuation present in the Lig5-PI3 K complex when contrasted with the pictilisib-PI3 K complex.

Analysis of protein and ligand interaction

Throughout the simulation, it is possible to monitor protein interactions with the ligand. These interactions are classifiable by type and can be summarized, as depicted in the plot above. Protein-ligand interactions, also referred to as "contacts," fall into four main categories: hydrogen bonds, hydrophobic, ionic, and water bridges. Each interaction type encompasses more detailed subtypes, which are accessible for exploration through the "Simulation Interactions Diagram" panel (Figure 8).

During the normalized trajectory of the PI3 K-pictilisib complex, it was observed that a sole amino acid, N853, sustained specific interactions for 50% of the simulation duration, whereas S854 retained only 30% (Figure 8A), both starting from 50 ns (Figure 8C). In contrast, none of the other residues maintained interactions exceeding 20% throughout the simulation period (Figure 8A and C).

While the PI3 K-Lig5 complex contained three amino acids, namely Y836, N853, and S854, it maintained more than 70% of the simulation time, with specific interactions maintained; thus, the residue V851 maintained interactions throughout the
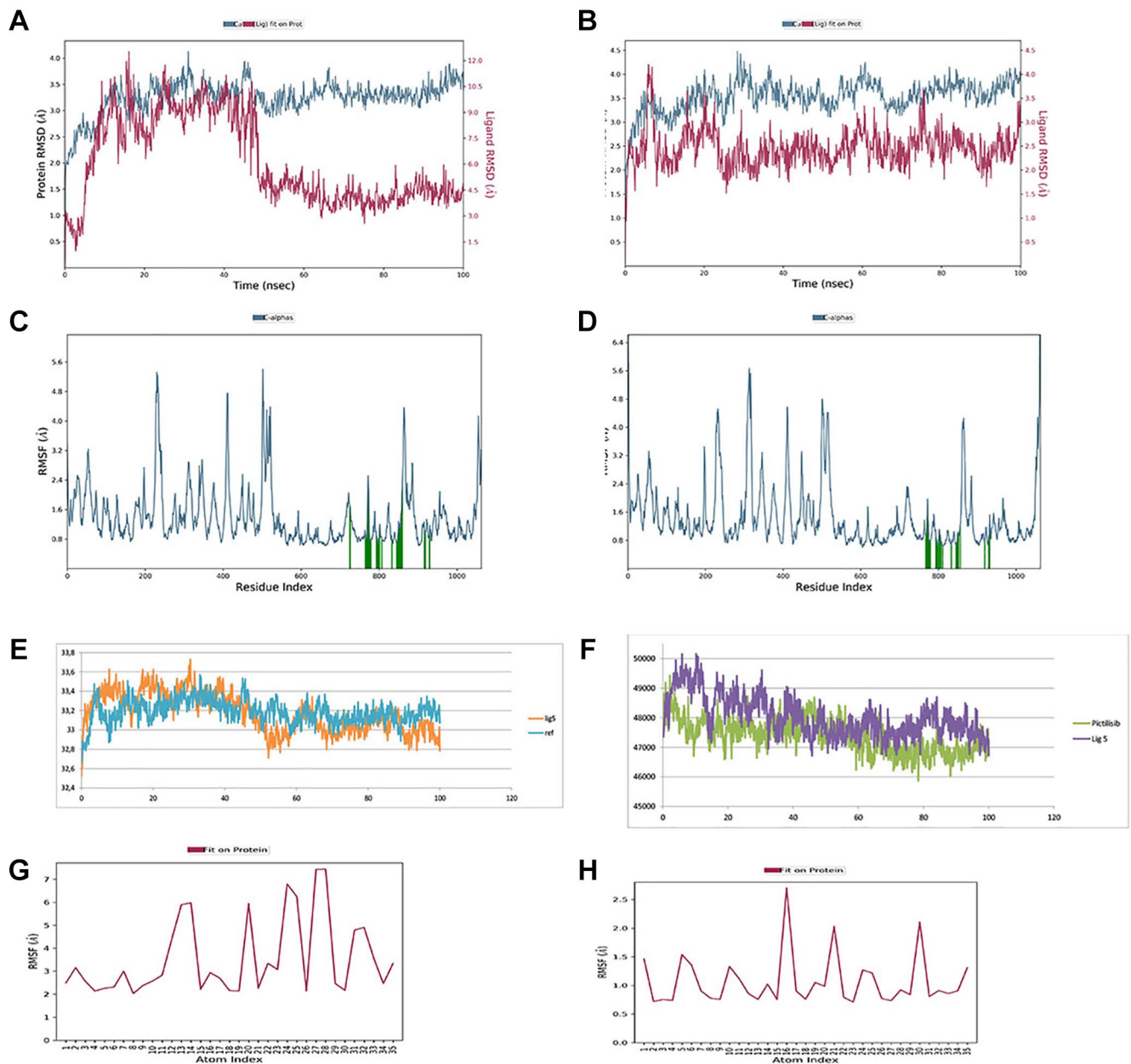
Figure 7. Molecular dynamics analysis of pictilisib-PI3 K and Lig5-PI3 K complexes: (A) RMSD of pictilisib-PI3 K complex; (B) RMSD of Lig5-PI3 K complex; (C) root mean square fluctuation (RMSF) of pictilisib-PI3 K complex; (D) RMSF of Lig5-PI3 K complex; (E) gyration of Lig5-PI3 K and pictilisib-PI3 K complexes; (F) solvent accessible surface area (SASA) of Lig5-PI3 K and pictilisib-PI3 K complexes; (G) RMSF of pictilisib; (H) RMSF of Lig5.

simulation, with a fraction of 1.75 (values over 1.0), which means that this residue establishes several contacts of the same subtype with the ligand (Figure 8B and D).

We also notice that the total number of contacts during the simulation is greater for Lig5 than for pictilisib, and these results are confirmed in the 2D diagram of interactions lasting more than 30% of the simulation time, showing that pictilisib has only one hydrogen bond with residue N853 while Lig5 establishes five hydrogen bonds including two with V851, as well as hydrophobic interactions and water bridges with other residues (Table 9).

Discussion

The PI3 K/Protein Kinase B(AKT)/Mammalian Target of Rapamycin (m-TOR) signaling pathway is known to be the most frequently altered pathway in the majority of human cancers. PI3 K dimeric lipid kinases are typically activated by RTKs, the phosphorylation of which allows recruitment of PI3 K to the plasma membrane via direct binding of p85 to the intracellular domain of the RTK or indirect binding through adapters. This results in a depression of the activity of the kinase p110, which phosphorylates PIP2 on the plasma membrane to generate PIP3.[41] Mutations in the
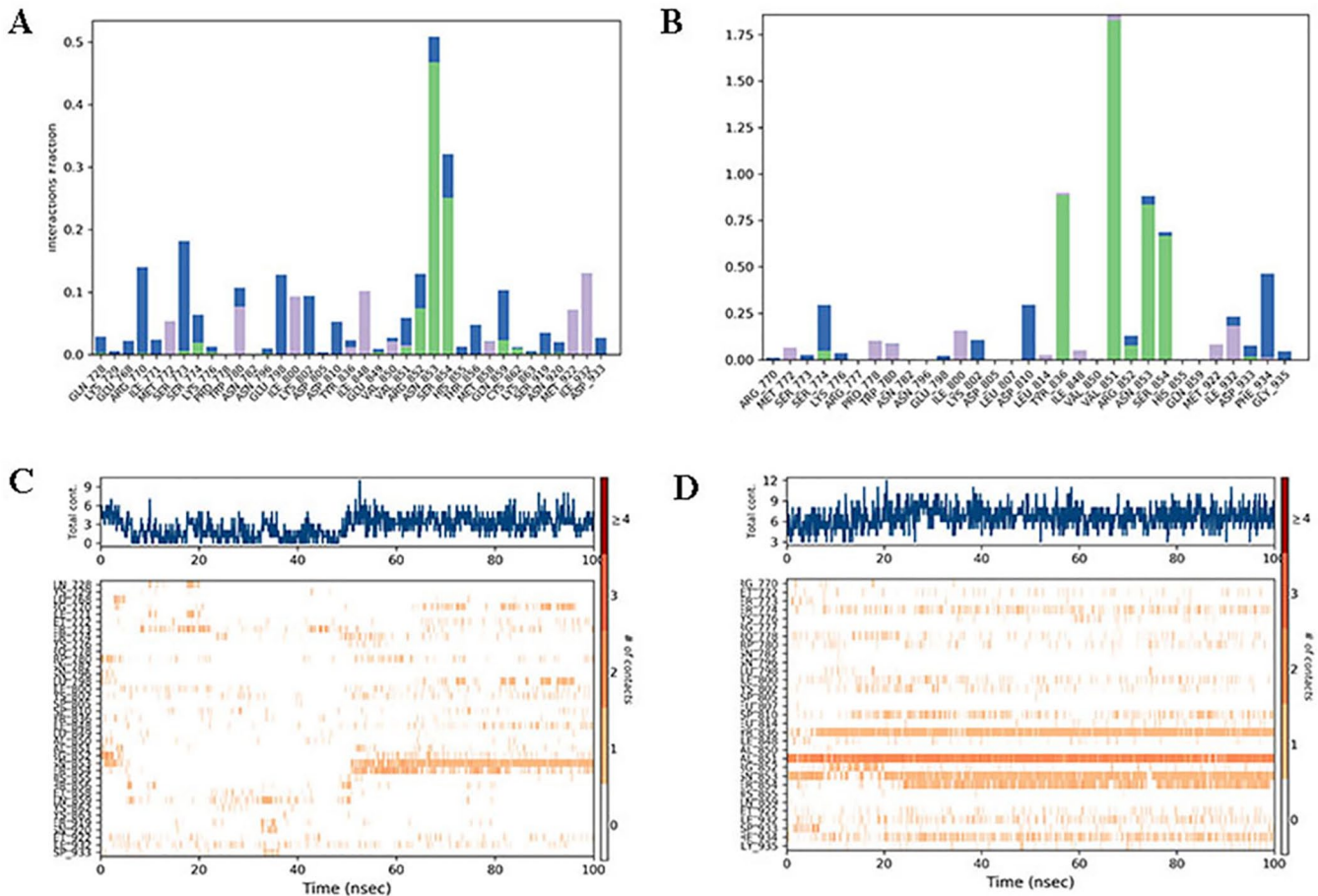
Figure 8. (A) Histogram of the protein-ligand complex of pictilisib and PI3K protein. (B) Histogram of the protein-ligand complex of Lig5 and PI3K protein. (C) Protein-ligand contact timeline plot of pictilisib bound to PI3K protein. (D) Protein-ligand contact timeline.

PIK3CA p110α catalytic subunit of PI3K have been strongly associated with altered protein product implicated in several types of cancer in humans.[10] What drew our attention to this protein is its consideration as a relevant target for the development of targeted therapies using computer-aided drug design.

Virtual screening is described as a sequential multi-step method, which goes through different selection criteria, from which the selection of compounds that can be developed into drugs with the desired biological activity is gradually reduced. The compounds under investigation do not need to be readily available, and their bioactivities are virtually predicted, saving expense and material. Therefore, any compound can be evaluated through virtual screening. Depending on the level of the study, the compound database for virtual screening can reach tens of millions of compounds, and all these compounds can be analyzed in a single screen.[42]
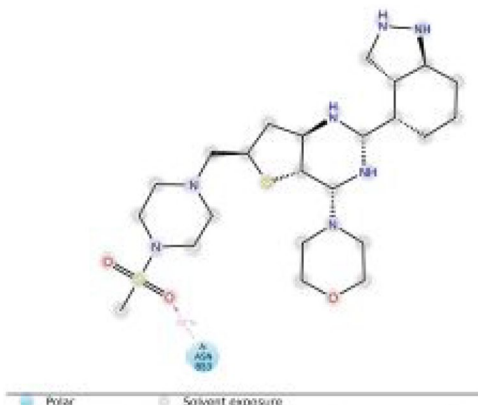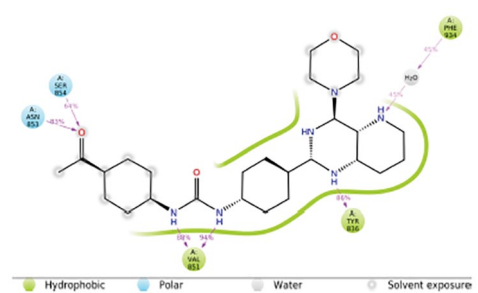
Based on these methods, it was possible to characterize 31 mutations of the PIK3CA gene affecting the function of the protein (10 mutations in breast cancer, 22 mutations in endometrial cancer, 5 mutations in colon cancer, and 1 mutation in ovarian cancer). Our results are consistent with the frequency of genetic alterations of the PI3K gene in cancer already published showing breast cancer with a frequency of 29.06%, endometrial cancer 27.62%, colorectal cancer 14.09%, and ovarian cancer 11.92%.[43]

VanLandingham et al[44] classified mutations affecting the PIK3CA gene into two categories: canonical mutations that occur in three hot spots—E542(K/A/G/Q/V) and E545(K/G/Q/ D/A/V) located in the helical domain (exon 9) and H1047(R/L/Y/Q/C) located in the kinase domain (exon 20)—and non-canonical mutations that occur at a multitude of sites and are distributed over the entire p110α sequence. However, in our study, apart from E545 V mutations in breast and colon cancer and E542 V in endometrial cancer, canonical mutations did not appear to affect protein function as predicted by SIFT, Polyphene-2, and MutPred2.

Although most studies imply that mutations in the *PIK3CA* gene in several types of cancer occur in the E542, E545, and H1047 sites, a study that was carried out on a cohort of 60 patients with hormone receptor positive (HR+)metastatic breast cancer detected another hot spot mutation "P539R." The latter was expressed with a high frequency in the primary tumor site (11.1%, 3/27 sample analyzed), in the circular DNA (16.1%, 5/31 sample analyzed), or in the cells circulatory tumors (23.1%, 6/26 sample analyzed).[45] Our data show that

Table 9. Two-dimensional interaction diagrams of titular compounds with a summary of all non-bounding interactions.

LIGAND	IUPAC NAME	2D LIGAND-INTERACTION DIAGRAM	INTERACTION
Pictilisib	4-(2-[1 *H*-indazol-4-yl)-6-[[4-methylsulfonylpiperazin-1-yl]methyl)thieno[3,2-d]pyrimidine-4-yl]morpholine		H-bond—ASN 853
Lig5	1-(4-acetylphenyl)-3-[4-(4-morpholin-4-ylpyrido[3,2-d]pyrimidine-2-yl)phenyl]urea		H-bond—VAL851(2), SER854, ASN853, TYR836 Hydrophobic interactionVAL851, TYR836, PHE,934 Water interaction PHE,934

the same mutation is deleterious in breast cancer as well as in endometrial cancer.

According to our results, we note that the four mutations, C901 F, P539R, G914R, and E600 K, are involved in both breast and endometrial cancer, while the E545 V mutation is linked to breast and colon cancer.

In addition, the results of the screening show that "Y1021 C" was the only deleterious mutation to be repeated in three types of cancer (breast cancer, endometrial cancer, and colon cancer). However, in a study by Shazia Bashir et al[46] on molecular alterations of PIK3CA in uterine carcinosarcoma, clear cell tumors, and serous tumors, this mutation appears in 14 out of 41 patients with uterine serous carcinoma (cancer of the type II endometrium). This may support the hypothesis proposed previously: "The Y1021 C mutation represents a hot spot in the p110α coding sequence." Apparently, other research implies that combinations of mutations located in different domains of p110α often have a synergistic effect (gain of function [GOF]), but combinations of mutations in the same domain are simply additive. This study indicated that the E545 K/Y1021 C mutation pair induces a loss of function when introduced into the same molecule, revealing an incompatibility between the combined changes induced by the mutations and the function of the p110α protein.[47]

The study of the impact of 31 deleterious mutations on the stability and flexibility of the PI3 K protein showed all the mutations significantly increase the stability and decrease the flexibility except the mutations L658 F, F684 L, F1002 L,

Y1021 C, and Y1021 H, which decrease these two settings with G914R, causing the greatest decrease in flexibility, and E600 V, increasing stability the most.

The effect of a mutation is described as a change in the specificity (selectivity) of the interactions between the mutated protein and its specific interactions: proteins, nucleic acids, or small molecules. This is due to a set of free energies of interactions between a given protein and all other proteins and ligands.[48]

Knowing that stability is the fundamental property that improves function,[49] for the majority of stability-enhancing mutations, the functional impact is a GOF, which can result from a change in the specificity of interactions with particular protein-substrate or a change in the specificity of interactions with regulatory proteins. Since our mutations studied are in the helical domain and the kinase domain, we then assume changes in the free energies of interaction with the native binders, which is ATP.[48]

For L658 F, F684 L, F1002 L, Y1021 C, and Y1021 H, a change in the flexibility pattern of functional residues could alter the functional region and activity of mutant proteins, and a decrease in overall flexibility and an increase in stiffness due to mutations can affect protein-binding properties causing a GOF.[49]

To demonstrate the impact of the mutation on the interaction with the reference drugs, mutated models of the PI3 K protein were generated and used to perform molecular docking with the reference drugs and then with collected compounds

meeting the Lipinski and Veber criteria and predicted to be non-toxic.

The inhibitors that we have chosen as reference have an important biological activity validated by several studies, except that alpelisib (R4) and copanlisib (R2) proved to be toxic elements according to the toxicity test that we have accomplished. In fact, hyperglycemia is known to be the primary adverse effect for HR+ and HER2-positive breast cancer patients with a mutated PIK3CA gene treated with alpelisib in clinical trials, with an absolute risk random effect of 59%. With the exception of hyperglycemia, treatment-emergent adverse events with alpelisib in clinical trials were generally low grade.[50] On the other hand, inavolisib was the best of the inhibitors in terms of physico-chemical properties, with a good IC50 value of 0.038 nM and a polar surface of 112 Å. These indices, in addition to the fact that it is not toxic, will make the latter an inhibitor promoter of PI3Kα.

The multi-docking that was carried out made it possible to test the affinity of 16 inhibitors (12 potential inhibitors + 4 reference inhibitors) for 32 targets including the 31 mutations and the wild-type "7PG5" using Autodock Vina. Among the reference inhibitors, pictilisib was the one with the best affinity for the majority of targets, and it is interesting to note that several mutations showed a positive effect following interactions with copanlisib, with a higher affinity than that of the wild type.

The results indicate that the Lig5 inhibitor (CID137641601) shows a significantly high affinity for the wild type or the different mutations of the PIK3CA gene in the four types of cancers studied, with values that vary between −9 and −9.3 kcal/mol. These values greatly exceed those of the reference inhibitors, which may make this inhibitor a strong and non-toxic drug candidate for the treatment of solid tumors representing excessive activity of the PI3Kα protein following an alteration at the gene level.

Apparently, Lig8 (CID137656901) may be proposed as a better choice for patients with endometrial cancer characterized by the presence of the M1004R, M1004V, S576Y, or E542V mutations. This is due to the increased affinity of Lig8 for these mutations, which were −9.4, −9.5, −9.4, and −9.4 kcal/mol, respectively. A positive effect was observed after its interaction with Lig8, with a very good affinity (−9.3 kcal/mol) exceeding that of the wild type (−9 kcal/mol).

Lig4 (CID137637213) and Lig12 (CID155512538) ligands can also be considered as relevant drug candidates for the treatment of breast, colon, and ovarian cancer.

On the other hand, in endometrial cancer, there were two mutations, "F1002L" and "E600V," with negative effect in which the affinity of Lig12 especially decreased in a remarkable way compared to the wild type and other mutations.

The ligand closest to the pharmacophore model is Lig1 with an RMSD score of 0.30, sharing common structures with the reference ligands used in generating the pharmacophore map. This may explain the close affinity exhibited by Lig1 and

the reference ligand pictilisib with wild-type PI3K, as well as the mutant model. However, Lig5, which demonstrated a higher affinity with wild-type PI3K and the mutant model compared to the reference inhibitors is less aligned with the generated pharmacophore than Lig1, with an RMSD of 0.40. Consequently, it presents a structure less akin to the reference inhibitors, exhibiting a structural uniqueness that allows this ligand to establish a strong affinity with the receptor.

In this context, the interaction between the reference inhibitor pictilisib and Lig5 with wild-type PI3K and the Y1021C mutant model indicates that the latter is more potent.

The unique binding interactions observed between Lig5 and the protein provide valuable insights into its enhanced affinity compared to the reference inhibitor, pictilisib. Lig5 establishes two hydrogen bonds with the protein, forming a strong connection with the S854 and V851 residues. In addition, a hydrogen bond is formed with the K802 residue, contributing further to the ligand's stability within the binding site. Furthermore, the presence of a pi-sulfur interaction with the C838 residue enhances the ligand's specificity for the protein. One notable feature is the pi-pi T-shaped interaction between Lig5 and W780, a residue critical for stabilizing ligand binding. This specific interaction augments the ligand's potency, creating a robust binding environment. Moreover, the ligand forms a pi-alkyl interaction with I932, showcasing its adaptability to diverse molecular environments. Another pi-alkyl interaction with I848 further contributes to the ligand's structural uniqueness, highlighting its ability to establish multiple stabilizing contacts.

Contrastingly, the reference inhibitor primarily relies on five pi-alkyl interactions, with one each at I800, I848, and V851 and two with I932, as well as three T-shaped pi-pi interactions, including Y836 and W780. In summary, the binding profile of Lig5, characterized by diverse interactions including hydrogen bonding, pi-sulfur, pi-pi T-shaped, and pi-alkyl, contributes to its enhanced efficacy in binding to the protein. The specific contacts with key residues emphasize the ligand's adaptability and structural uniqueness, which collectively result in a more potent binding affinity compared to the reference inhibitor, pictilisib.

In the present research, MD simulation was performed for the best ligand (Lig5) compared to the standard pictilisib-PI3Ka complex. After analyzing the simulation interaction diagram data, it was observed that the RMSD of the Lig5-PI3K ligand complex exhibits fluctuations of 2 to 3 Å, which is very stable and within the acceptable range (1-4 Å)[51] in the specific binding pocket of PI3K; thus, the complex did not show a significant deviation from the initial position during MD analysis, meaning that the binding is stable, while the pictilisib-PI3K complex exhibits fluctuations from 4.5 to 10.5 Å relative to the initial frame throughout the trajectory, at the start of the simulation from 0 up to 40 ns, the complex showed instability with an RMSD of 10.5 Å and only started to

stabilize after 40 ns with an RMSD of 4.5 Å still remaining outside the acceptable range (1-4 Å).[51]

The compactness and dynamic stability of both systems were assessed using the radius of gyration (Rg) after ligand binding, offering insights into the structural alterations of the protein throughout the simulation. Rg values were computed over a 100-ns trajectory and juxtaposed with the simulation duration depicted in Figure 7E. Analysis revealed that the lig5-PI3 K system initially exhibited a notably higher Rg value than the pictilisib-PI3 K complex, but this trend reversed after the first 40 ns. Initially, the lig5-PI3 K system displayed commendable compactness (33.5 ± 0.3 Å); however, after 40 ns, the Rg value gradually decreased to 33.0 ± 0.3 Å. During this interval, Lig5 assumed a specific position, leading to reduced fluctuation, a finding corroborated by the relatively stable RMSD compared to the alternate system. Conversely, the pictilisib-PI3 K system exhibited fewer structural variations and maintained an overall stable Rg value (33.18 ± 0.12 Å).

The SASA values for Lig5-PI3 K and pictilisib-PI3 K were recorded as 48032.97 A ± 690.36 and 47387.95 A ± 557.28, respectively. Each complex's average SASA value underwent statistical validation. Throughout the 100-ns MD simulations, both complexes experienced a notable decrease in SASA values, suggesting structural modifications within the protein. The Lig5-PI3 K complex exhibited a higher SASA value than the pictilisib-PI3 K complex, indicating the unfolding of PI3 K's compact structure upon binding with ligand 5, thereby allowing water molecules to permeate the newly exposed pocket.

The mean RMSF of Lig5 was 1.07 Å, whereas the average RMSF for pictilisib was 3.55 Å (Figure 7G and H). This suggests a lower level of fluctuation observed in the Lig5-PI3 K complex than in the pictilisib-PI3 K complex. These findings imply a more stable ligand-protein complex, affirming that Lig5, as a competitive inhibitor, exhibited superior performance compared to pictilisib in binding to the protein.

During the normalized trajectory of the PI3 K-pictilisib complex, N853 sustained specific interactions for 50% of the simulation duration, while S854 retained only 30%. Conversely, none of the other residues maintained interactions exceeding 20% throughout the simulation period. In contrast, the PI3 K-Lig5 complex exhibited more robust interactions, with W836, N853, and S854 maintaining over 70% of the simulation time with specific interactions. In addition, V851 sustained interactions throughout the simulation, with a fraction of 1.75, indicating multiple contacts of the same subtype with the ligand.

From this analysis, it seems that the PI3 K-Lig5 complex has stronger and more sustained interactions with the specific residues mentioned compared to the PI3 K-pictilisib complex. The differences in interactions between the complexes may have implications for their binding affinities, biological activities, and potential therapeutic applications. These molecules exhibit distinct chemical compositions and structures. The pictilisib molecule features a urea core with two aromatic rings: one being 4-acetylphenyl and Lig5, a complex structure

comprising a pyrido[3,2-d]pyrimidine ring attached to a phenyl ring with a morpholin-4-yl substituent. Both molecules also contain nitrogen-containing heterocycles, such as pyrimidine. This fused nitrogen-based heterocycle serves as an isostere to the adenine ring found in ATP, enabling these molecules to emulate crucial hinge region-binding interactions within kinase active sites.[52] Targeted chemical modifications can effectively guide the activity and specificity of pyrazolo[3,4-d] pyrimidines toward PI3 K, and there are four possible isomeric pyridopyrimidines.[53,54] One among them are the pyrido[2,3-d] pyrimidines known for their biological activity as kinase inhibitors and antitumor agents,[55] and this is the case of the predicted non-toxic Lig5 which showed a very good interaction in our studies with the wild PI3 K kinase and with different mutated models involved in different types of cancer, validated by MD, which is proposed as a potential inhibitor against PI3 K and could act with different mutational profiles, thus overcoming the problem of resistance and toxicity.

Conclusion

Our study sheds light on the diverse landscape of PIK3CA mutations across multiple cancer types and their implications for therapeutic interventions targeting PI3Kα. Through virtual screening, molecular docking, and MD simulations, we identified Lig5 as a potent inhibitor with promising specificity and non-toxic properties. MD simulations further affirmed Lig5's stability and robust interactions with PI3 K, suggesting its potential as a versatile therapeutic agent capable of overcoming resistance issues. Overall, our findings provide valuable insights for the development of targeted therapies against PI3 K-driven cancers, offering a pathway toward personalized and effective treatment strategies.

Author Contributions

Ilham Kandoussi: Study conception and design, data acquisition, analysis and interpretation, writing and critical revision of the article. Ghyzlane El Haddoumi: Acquisition and interpretation of data, writing of the article. Mariam Mansouri: Data acquisition and analysis. Lahcen Belyamani: Critical revision of the article. Azeddine Ibrahimi: Study design and supervision. Rachid Eljaoudi: Final approval of the version to be submitted.

ORCID iD

Ilham Kandoussi [iD] https://orcid.org/0000-0002-5894-7817

REFERENCES

1. Ligresti G, Militello L, Steelman LS, et al. PIK3CA mutations in human solid tumors. *Cell Cycle*. 2009;8:1352-1358. doi:10.4161/cc.8.9.8255
2. Vivanco I, Sawyers CL. The phosphatidylinositol 3-kinase–AKT pathway in human cancer. *Nat Rev Cancer*. 2002;2:489. doi:10.1038/nrc839
3. Liu P, Cheng H, Roberts TM, Zhao JJ. Targeting the phosphoinositide 3-kinase pathway in cancer. *Nat Rev Drug Discov*. 2009;8:627-644. doi:10.1038/nrd2926
4. Vanhaesebroeck B, Guillermet-Guibert J, Graupera M, Bilanges B. The emerging mechanisms of isoform-specific PI3K signalling. *Nat Rev Mol Cell Biol*. 2010;11:329-341. doi:10.1038/nrm2882

5. Liu X, Xu Y, Zhou Q, et al. PI3K in cancer: its structure, activation modes and role in shaping tumor microenvironment. *Future Oncol*. 2018;14:665-674. doi:10.2217/fon-2017-0588

6. Ciriello G, Miller ML, Aksoy BA, Senbabaoglu Y, Schultz N, Sander C. Emerging landscape of oncogenic signatures across human cancers. *Nat Genet*. 2013;45:1127-1133. doi:10.1038/ng.2762

7. Samuels Y, Velculescu VE. Oncogenic mutations of PIK3CA in human cancers. *Cell Cycle Georget Tex*. 2004;3:1221-1224. doi:10.4161/cc.3.10.1164

8. Zhao L, Vogt PK. Helical domain and kinase domain mutations in p110alpha of phosphatidylinositol 3-kinase induce gain of function by different mechanisms. *Proc Natl Acad Sci U S A*. 2008;105:2652-2657. doi:10.1073/pnas.0712169105

9. Levine DA, Bogomolniy F, Yee CJ, et al. Frequent mutation of the PIK3CA gene in ovarian and breast cancers. *Clin Cancer Res*. 2005;11:2875-2578. Accessed May 18, 2023. https://pubmed.ncbi.nlm.nih.gov/15837735/

10. Alqahtani A, Ayesh HSK, Halawani H. PIK3CA gene mutations in solid malignancies: association with clinicopathological parameters and prognosis. *Cancers*. 2019;12:93. doi:10.3390/cancers12010093

11. Willis O, Choucair K, Alloghbi A, et al. PIK3CA gene aberrancy and role in targeted therapy of solid malignancies. *Cancer Gene Ther*. 2020;27:634-644. doi:10.1038/s41417-020-0164-0

12. Gustin JP, Cosgrove DP, Park BH. The PIK3CA gene as a mutated target for cancer therapy. *Curr Cancer Drug Targets*. 2008;8:733-740. doi:10.2174/156800908786733504

13. Mishra R, Patel H, Alanazi S, Kilroy MK, Garrett JT. PI3K inhibitors in cancer: clinical implications and adverse effects. *Int J Mol Sci*. 2021;22:3464. doi:10.3390/ijms22073464

14. Castel P, Toska E, Engelman JA, Scaltriti M. The present and future of PI3K inhibitors for cancer therapy. *Nat Cancer*. 2021;2:587-597. doi:10.1038/s43018-021-00218-4

15. Roulot A, Héquet D, Guinebretière JM, et al. Tumoral heterogeneity of breast cancer. *Ann Biol Clin (Paris)*. 2016;74:653-660. doi:10.1684/abc.2016.1192

16. Juric D, Rodon J, Tabernero J, et al. Phosphatidylinositol 3-kinase α–selective inhibition with alpelisib (BYL719) in PIK3CA-altered solid tumors: results from the first-in-human study. *J Clin Oncol*. 2018;36:1291-1299. doi:10.1200/JCO.2017.72.7107

17. ClinVar. Accessed May 19, 2023. https://www.ncbi.nlm.nih.gov/clinvar/

18. The Cancer Genome Atlas Program (TCGA)—NCI. Published May 13, 2022. Accessed May 19, 2023. https://www.cancer.gov/ccg/research/genome-sequencing/tcga

19. Berman HM, Westbrook J, Feng Z, et al. The protein data bank. *Nucleic Acids Res*. 2000;28:235-242. doi:10.1093/nar/28.1.235

20. Chen JE, Huang CC, Ferrin TE. RRDistMaps: a UCSF Chimera tool for viewing and comparing protein distance maps. *Bioinforma Oxf Engl*. 2015;31:1484-1486. doi:10.1093/bioinformatics/btu841

21. Pejaver V, Urresti J, Lugo-Martinez J, et al. Inferring the molecular and phenotypic impact of amino acid variants with MutPred2. *Nat Commun*. 2020;11:5918. doi:10.1038/s41467-020-19669-x

22. Ng PC, Henikoff S. SIFT: predicting amino acid changes that affect protein function. *Nucleic Acids Res*. 2003;31:3812-3814. Accessed May 18, 2023. https://www.ncbi.nlm.nih.gov/pmc/articles/PMC168916/

23. Adzhubei I, Jordan DM, Sunyaev SR. Predicting functional effect of human missense mutations using PolyPhen-2. *Curr Protoc Hum Genet*. 2013;Chapter7:Unit720. doi:10.1002/0471142905.hg0720s76

24. Rodrigues CH, Pires DE, Ascher DB. DynaMut: predicting the impact of mutations on protein conformation, flexibility and stability. *Nucleic Acids Res*. 2018;46:W350-W355. doi:10.1093/nar/gky300

25. Demir Cetinkaya B, Biray Avci C. Molecular perspective on targeted therapy in breast cancer: a review of current status. *Med Oncol Northwood Lond Engl*. 2022;39:149. doi:10.1007/s12032-022-01749-1

26. Huang TT, Lampert EJ, Coots C, Lee JM. Targeting the PI3K pathway and DNA damage response as a therapeutic strategy in ovarian cancer. *Cancer Treat Rev*. 2020;86:102021. Accessed June 2, 2023. https://www.ncbi.nlm.nih.gov/pmc/articles/PMC7272282/

27. Han N, Jiang Y, Gai Y, et al. 11C-labeled pictilisib (GDC-0941) as a molecular tracer targeting phosphatidylinositol 3-kinase (PI3K) for breast cancer imaging. *Contrast Media Mol Imaging*. 2019;2019:1760184. doi:10.1155/2019/1760184

28. El Haddoumi G, Mansouri M, Bendani H, et al. Facing antitubercular resistance: identification of potential direct inhibitors targeting InhA enzyme and generation of 3D-pharmacophore model by in silico approach. *Adv Appl Bioinform Chem*. 2023;16:49-59. doi:10.2147/AABC.S394535

29. Haddoumi GE, Mansouri M, Bendani H, et al. Selective non-toxics inhibitors targeting DHFR for tuberculosis and cancer therapy: pharmacophore generation and molecular dynamics simulation. *Bioinform Biol Insights*. 2023;17:11779322231171778. doi:10.1177/11779322231171778

30. Borba JVB, Alves VM, Braga RC, et al. STopTox: an in silico alternative to animal testing for acute systemic and topical toxicity. *Environ Health Perspect*. 2022;130:27012. doi:10.1289/EHP9341

31. Bhaskar BV, Rammohan A, Babu TM, et al. Molecular insight into isoform specific inhibition of PI3K-α and PKC-η with dietary agents through an ensemble pharmacophore and docking studies. *Sci Rep*. 2021;11:12150. doi:10.1038/s41598-021-90287-3

32. Trott O, Olson AJ. AutoDock Vina: improving the speed and accuracy of docking with a new scoring function, efficient optimization and multithreading. *J Comput Chem*. 2010;31:455-461. doi:10.1002/jcc.21334

33. Goodsell DS. Computational docking of biomolecular complexes with AutoDock. *Cold Spring Harb Protoc*. 2009;2009(5):pdb.prot5200. doi:10.1101/pdb.prot5200

34. Khedkar SA, Malde AK, Coutinho EC, Srivastava S. Pharmacophore modeling in drug discovery and development: an overview. *Med Chem*. 2007;3:187-197. doi:10.2174/157340607780059521

35. Scalable algorithms for molecular dynamics simulations on commodity clusters. Paper presented at: 2006 ACM/IEEE conference on supercomputing. doi:10.1145/1188455.1188544

36. Ferreira LG, Dos Santos RN, Oliva G, Andricopulo AD. Molecular docking and structure-based drug design strategies. *Mol Basel Switz*. 2015;20:13384-13421. doi:10.3390/molecules200713384

37. Hildebrand PW, Rose AS, Tiemann JKS. Bringing molecular dynamics simulation data into view. *Trends Biochem Sci*. 2019;44:902-913. doi:10.1016/j.tibs.2019.06.004

38. Rasheed MA, Iqbal MN, Saddick S, et al. Identification of lead compounds against Scm (fms10) in enterococcus faecium using computer aided drug designing. *Life Basel Switz*. 2021;11:77. doi:10.3390/life11020077

39. Shivakumar D, Williams J, Wu Y, Damm W, Shelley J, Sherman W. Prediction of absolute solvation free energies using molecular dynamics free energy perturbation and the OPLS force field. *J Chem Theory Comput*. 2010;6:1509-1519. doi:10.1021/ct900587b

40. Padmanabhan D, Siddiqui MH, Natarajan P, Palanisamy S. Hecogenin a plant derived small molecule as an antagonist to BACE-1: a potential target for neurodegenerative disorders. *Metabolites*. 2023;13:758. doi:10.3390/metabo13060758

41. Jiang W, Ji M. Receptor tyrosine kinases in PI3K signaling: the therapeutic targets in cancer. *Semin Cancer Biol*. 2019;59:3-22. doi:10.1016/j.semcancer.2019.03.006

42. Virtual screening strategies in drug discovery—a brief overview. *Vietnam J Sci Technol*. 2021;59:415-440. Accessed June 6, 2023. https://vjs.ac.vn/index.php/jst/article/view/16003

43. Papas Y, Asmar AE, Ghandour F, Hajj I. Malignant phyllodes tumors of the breast: a comprehensive literature review. *Breast J*. 2020;26:240-244. doi:10.1111/tbj.13523

44. VanLandingham NK, Nazarenko A, Grandis JR, Johnson DE. The mutational profiles and corresponding therapeutic implications of PI3K mutations in cancer. *Adv Biol Regul*. 2023;87:100934. doi:10.1016/j.jbior.2022.100934

45. Patients with metastatic hormone receptor-positive breast cancer express PIK3CA oncogene mutational heterogeneity in circulating tumor cells. Accessed June 6, 2023. https://www.semanticscholar.org/paper/Patients-with-metastatic-hormone-receptor-positive-Laere-Peeters/900c52c5d62ec331f888a0a7776df27bd4b0b9b4

46. Bashir S, Jiang G, Joshi A, et al. ATL. *Int J Gynecol Cancer*. 2014;24(7):1262-1267. doi:10.1097/IGC.0000000000000183

47. Vogt PK, Hart JR, Gymnopoulos M, et al. Phosphatidylinositol 3-kinase (PI3K): the oncoprotein. *Curr Top Microbiol Immunol*. 2011;347:79-104. doi:10.1007/82_2010_80

48. Reva B, Antipin Y, Sander C. Predicting the functional impact of protein mutations: application to cancer genomics. *Nucleic Acids Res*. 2011;39:e118. doi:10.1093/nar/gkr407

49. N N, Zhu H, Liu J, et al. Analysing the effect of mutation on protein function and discovering potential inhibitors of CDK4: molecular modelling and dynamics studies. *PLoS ONE*. 2015;10:e0133969. doi:10.1371/journal.pone.0133969

50. Tankova T, Senkus E, Beloyartseva M, et al. Management strategies for hyperglycemia associated with the α-selective PI3K inhibitor alpelisib for the treatment of breast cancer. *Cancers*. 2022;14:1598. doi:10.3390/cancers14071598

51. Halder D, Das S, R A, R S J. Molecular docking and dynamics based approach for the identification of kinase inhibitors targeting PI3Kα against non-small cell lung cancer: a computational study. *RSC Adv*. 2022;12(33):21452-21467. doi:10.1039/d2ra03451d

52. Baillache DJ, Unciti-Broceta A. Recent developments in anticancer kinase inhibitors based on the pyrazolo[3,4-d]pyrimidine scaffold. *RSC Med Chem*. 2020;11:1112-1135. doi:10.1039/d0md00227e

53. *Product Class 19: Pyridopyrimidines*. 2004th ed. Thieme Verlag; 2004. doi:10.1055/sos-SD-016-01443

54. Buron F, Mérour JY, Akssira M, Guillaumet G, Routier S. Recent advances in the chemistry and biology of pyridopyrimidines. *Eur J Med Chem*. 2015;95:76-95. doi:10.1016/j.ejmech.2015.03.029

55. Jubete G, Puig de la Bellacasa R, Estrada-Tejedor R, Teixidó J, Borrell JI. Pyrido[2,3-d]pyrimidin-7(8H)-ones: synthesis and biomedical applications. *Molecules*. 2019;24:4161. doi:10.3390/molecules24224161